Acta Physica Universitatis Comenianae
Vol. L–LI, Number 1&2 (2009–2010) 53–65

A Model for Simulation of High-Energy Nucleon-Nucleus Collision*

J. Husár[1], J. Masarik[1], P. Musil[2]

[1]Department of Nuclear Physics, Faculty of Mathematics, Physics and Informatics, Comenius University, Mlynská dolina F/1, SK – 842 48 Bratislava, Slovakia
[2]Slovak Health University, Limbová 12, 833 03 Bratislava, Slovakia

Abstract: A method for calculation of high-energy hadron-nucleus interaction based on Monte Carlo simulations of cascade and evaporation process is described. The results of the simulations are compared with other models and experimental data. The quantitative agreement between results of our calculations and experimental data indicates the necessity to improve the present model calculations mainly in respect to used cross sections.

1. Introduction

The interaction of high-energy particles with matter is of great interest in different areas, including nuclear physics, cosmic ray physics, radiation effects on materials, radiation hazards in space, biology and medicine.

It has been shown [1–4] that the mechanisms of collision of high-energy particle with complex nuclei can be divided into two stages. In the first stage of nuclear reaction an intranuclear cascade is initiated by the incoming particle. In this stage the reaction can be described in terms of particle-particle collisions with nucleus. These interactions are governed by the same cross sections that are applicable in the free space, but modified by Pauli exclusion effects inside the nucleus. The justification for this model is that the wavelength of the high-energy incoming particle and subsequent reaction products are of the order of or smaller than the average internucleon distance within the nucleus ($\sim 10^{-15}$ m). On the basis of this assumption one can simulate the intranuclear cascade by studying the behavior of individual particles within the nucleus.

The simulation of the cascade processes is started by a choice of primary particle characteristics. Then the point of collision, the type of collision and momenta of the produced particles are determined by Monte Carlo techniques. After the intranuclear cascade phase of interaction the residual nucleus is left in highly excited state. This nucleus is de-excited by particle emission that is commonly known as the evaporation process.

Many computer codes implementing cascade-evaporation model of high-energy collisions have been written [2–9]. They all have been realized by the Monte Carlo technique and quantitatively reproduced experimental data. In spite of this a new one has been written with the aim to improve the previous calculations in the sense of reduction of number of approximations made in previous treatments and utilization of more recent data on particle -particle interactions used as input data.

*) *Devoted to the 70th anniversary of Prof. Ján Pišút, Assoc. Prof. Martin Chudý and Assoc. Prof. Nevenka Pišútová.*

In this paper we report the basic physical features of our model for simulation of high-energy particle-nucleus interactions and comparison of results of calculations based on this model with existing experimental data and results of other calculations.

2. Nuclear Model

The first prerequisite for simulation of intranuclear cascade and evaporation processes is the specification of nuclear model in the frame of which calculations are realized. In our calculations, target nucleus is approximated by degenerate Fermi gas with the Fermi energy given by

$$E_F \quad \frac{\hbar^2}{2m}(3 \ ^2 \ _i)^{3/2} , \tag{1}$$

where m is the nucleon mass, index i stands for either neutron or proton and $_i$ is the density of protons and neutrons, respectively. The nuclear density distribution was considered in the form of step function that is depicted in Fig. 1. The Fermi energy at any point in the nucleus was computed from the corresponding density $_i$.

The form of nuclear density distribution was determined from the assumption that the shape of nuclear density distribution is identical with the shape of the measured [10] charge distribution that may be represented by the Fermi distribution

$$(r) \quad \frac{_0}{1 \quad e^{(r \ c)/a}} \tag{2}$$

with $c \quad 1.07 \quad A^{1/3} \quad 10^{\ 13}$ m and $r \quad r_{0.1} \quad r_{0.9} \quad 2.4 \quad 10^{\ 15}$ m, where $r_{0.1}$ and $r_{0.9}$ are the radii at which the density has dropped to 0.1 $_0$ and 0.9 $_0$, respectively. Seven concentric shells were used for the approximation of this distribution. The radii of the spheres have been determined as the distances at which the Fermi type charge distribution function reaches various fractions of the central maximum density. The outer radius of the central region is $c \quad 2.5 \quad 10^{\ 15}$m. The outermost region is $1.25 \quad 10^{\ 15}$m thick and its inner radius corresponds to the radius at which the density of the Fermi distribution has fallen to 10% of the maximum value $_0$. The same thickness has the first step from the top. The remaining regions have equal thickness. The value of the density of the outermost region $_0$ is determined by the condition that it contains the sphere of radius r in the Fermi distribution. The difference in the density between the central region (region 0) and the neighboring region is also equal to $_0$. The density differences between all intermediate regions are the same and equal to

$$(\ _0 \quad 2 \quad)/5 \tag{3}$$

The absolute value of quantity is determined from the normalization condition for the total nucleus mass. The nuclear density in the i-th region can be expressed as

$$_i \quad _0 \qquad (i \quad 1) , \tag{4}$$

where $I = 1, ..., 5$. The neutron to proton density ratio in each region was the same and was equal to the ratio of protons to neutrons within the nucleus $Z/(A - Z)$. Neutron or proton deficiencies at the nuclear surface below and above this ratio were not taken into account.

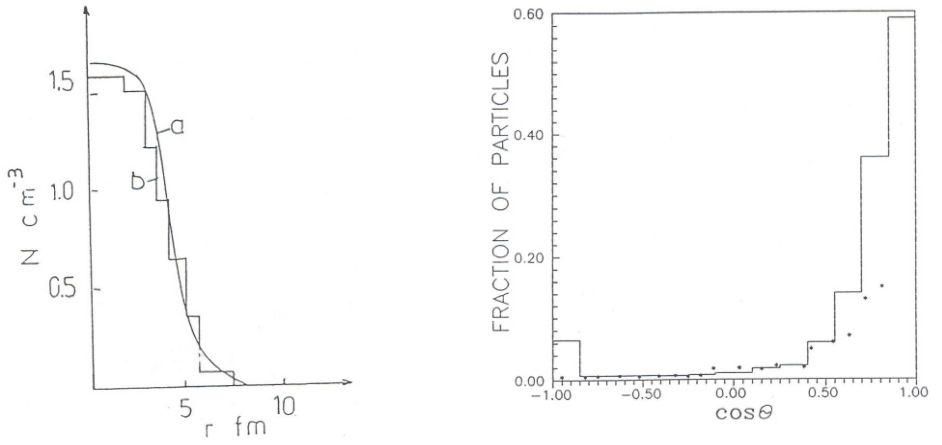

Fig. 1. Model of nuclear density distributions a) Fermi distribution; b) step function distribution.

The variation of nuclear density causes the variation of the Fermi energy and this leads to different values of nuclear potential of protons and neutrons within the various density regions. These changes were considered in the simulation of the cascade particle transport within the nucleus. It follows from the requirement of energy conservation that as the particles crossed the region boundaries they gained or lost kinetic energy in the amount in which the potential was changed. Besides the correction of kinetic energy of the cascade particles, the variations of nuclear potential necessitate the changes in direction of particle motion, as well. These are accounted for through the reflection and refraction of particles on boundaries of different nuclear density regions. These processes lead to the necessity of correction of radial component of the particle momentum on the boundaries of adjoined density regions. The tangential component remains unchanged. The angle of refraction is given by the equation

$$\frac{\sin}{\sin} \quad \frac{p}{p},$$

where p and p are the momenta of the cascade particles in the new and old density regions, respectively. The radial component of the new momentum can be expressed as follows

$$p_R \quad p_R^2 \quad E^2 \quad E^2,$$

where the new energy E is given by

$$E \quad E \quad (V \quad V),$$

where V and V are the values of the nuclear potential in new and old regions, respectively. The critical angle for total reflection follows from Equation (5) and (6) under the condition that sin

$$\cos \quad _{CR} \quad \frac{(E^2 \quad E^2)^{1/2}}{p}.$$

3. Particle-particle cross section data

The basic input parameters needed for cascade simulation are particle-particle cross sections of relevant physical processes. Only the nucleons and pions are interpreted as particles participating in the cascade development. The other particles (e.g. electrons) are taken into account from the point of view of energy conservation, only. The total cross section of *pn* and *np* interactions used in calculations and the data for production and absorption of pions in nucleon-nucleon (*NN*) and pion-nucleon (*N*) collisions are taken from papers [7, 11–15]. These cross sections, together with the information on properties and size of nucleus, were used for calculation of the mean free path of nucleons and pions within a nucleus and for simulation of production of secondary particles. At energies above 2 GeV, a triple-pion production is considered. The cross section for this process is taken to be by factor of 5 smaller than for the double production. The way in which resonance processes are incorporated into simulation is described below.

The *pp* and *np* differential cross sections were taken from the paper [4]. In the energy region where experimental data for *np* differential cross sections are not available, the shape of differential cross sections in the forward and backward directions was taken to be equal to the shape of *pp* cross section. The correction on the scattering directed into the backward hemisphere in the c.m. system as a function of energy [16] was also considered.

The cross sections for arbitrary energy in the model calculations were obtained by linear extrapolation and interpolation method applied to the above presented experimental input data. The extrapolation and interpolation were done in the first place as a function of energy at fixed angles and then as a function of angle at fixed energy. Experimental data are taken from [17].

The total inelastic hadron-nucleus cross sections can be represented as a sum over exclusive particle production cross sections. There are accurate and detailed experimental data [17–24]. A substantial contribution to the total cross section is due to a quasi-two-body reaction through one or two resonances. On the base of this, we assume in our calculations, that all inelastic reactions in the considered energy region can be represented by two-body interactions with single- or double-resonance production. Especially at lower energies the direct resonance production is considered too.

All production channels are considered, if they contribute more than 5% to the total inelastic cross section in our model. Only one direct resonance, which subsequently decay into three particles via one of the allowed channels, is taken into account near pionization threshold. The masses *M* of the decaying resonances are distributed with a decay-width according to formula given in [25].

The generation of an inelastic collision event with accounting resonance production is organized as follows:

1. Random selection of one reaction channel according to the tabulated cross sections for a given particle with specified properties.
2. Determination of kinematical variables of produced particles.
3. Decay of unstable particles and determination of properties of decay products. The isotropic distribution of products is supposed.
4. Relativistic transformation of the momenta and energies of all produced particles into the target nucleus rest frame.

Only nucleons and pions are considered for the development of higher generations of particles in the intranuclear cascade. The other particles are taken into account only for balance of collision from the point of view of energy, momentum, strangeness, charge and baryon number conservation.

4. Energy balance of collision

The development of the cascade process is followed until the energy of all produced particles drops below some cutoff value E_c. This value determines the separation between the cascade and evaporation stage of the calculation [26]. When the energy of cascade collision product with respect to the outside of the nucleus falls below the energy E_c, it is assumed that this particle can no longer escape from the nucleus as a cascade particle. It becomes a part of intermediate nucleus and its energy contributes to the excitation energy of the intermediate residual nucleus. This energy is the free parameter of the model and it may have a different value for proton and neutron at lower energies. In our calculations we used the same value for both neutrons and protons, equal to the sum of the Fermi energy, mean binding energy and Coulomb barrier. This value was calculated for the initial nucleus and has not been corrected during the development of the cascade process. The last statement holds for all the mean characteristics during development of cascade stage of high-energy particle-nucleus collision.

After the cascade stage of collision, the intermediate residual nucleus is usually left in the highly excited state. The excitation energy E_{Ex} is calculated as follows

$$E_{Ex} \quad (E_p \quad B_p) \quad B_N(A_p \quad _N) \quad \sum_{n,p} E_i \quad (E_i \quad m_i c^2) \quad E_R ,$$

where E_p is the kinetic energy of the projectile particle, B_p is the binding energy of the projectile (in the case of heavy ion collision with nucleus), B_N is the binding energy of nucleon with nucleus, $_N$ is the total number of nucleons produced in collision, E_i is the kinetic energy of the i type produced particle, $_{n,p}$, runs over all produced nucleons and pions, respectively, and E_R is the recoil energy of intermediate residual nucleus, which is determined by subtraction of momenta of all produced cascade particles from the momentum of incident particle. Momentum of the intermediate residual nucleus is determined in a similar way.

As the cascade and evaporation phase of collision are treated separately, the average values of the excitation energy, E_{Ex}, and the cascade energy (the total energy of cascade particles), E_{ca}, are needed as input parameters. These are determined by empirical functions of the kinetic energy, where parameters depend on the atomic number of the target nucleus. At incident momenta greater than 5 GeV/c, these values are used as the actual values in an individual collision. At lower energies, the actual values are sampled from appropriate truncated Gaussian distribution.

The excitation energy E_{Ex} is sampled from the Gaussian distribution with the mean value E_{Ex} and the width $E_{Ex} \quad 0.5 \quad E_{Ex}$ [27]

$$G(E) \quad \frac{1}{(2 \quad)^{1/2} \quad E_{ex}} e^{-(E_{ex} \quad \bar{E}_{ex})^2/2(\quad E_{ex})^2}, \qquad (5)$$

where E_{Ex} is determined by

$$\overline{E}_{ex} \quad \begin{array}{ll} T_0 & \text{for } T_0 \quad E_{Th} \\ E_{Th} \quad (T_0 \quad E_{Th})(B \quad E_{Th})(T_C \quad E_{Th}) & \text{for } E_{Th} \quad T_0 \quad T_C \\ B & \text{for } T_0 \quad T_C \end{array},$$

where T_0 is the projectile kinetic energy, E_{Th} is the threshold energy of pion production (128 MeV) and T_C and B are parameters [24]

$$\begin{aligned} T \quad & 3\,\text{GeV} \\ B \quad & \text{Max}(E_{Th}, \text{Min}((A^{1/3}/9 \quad 0.2), 0.01A)), \end{aligned} \tag{6}$$

where A is the atomic number of target nucleus.

The total energy of cascade particles, E_{ca}, is distributed according to the deformed Gaussian

$$G(E_{ca}) \quad \frac{1}{(2\ )^{1/2} \quad E_{ca}} e^{\ (E_{ca} \quad _{ca})^2/2(\ E_{ca})^2} \tag{7}$$

with the width $E_{ca} \quad B_{ca} \ _{ca}$, $B_{ca} \quad 0.5$ and the mean value $_{ca}$ which is the sum of the mean cascade energies of protons $^{(p)}_{ca}$ and neutrons $^{(n)}_{ca}$.

The mean values of the cascade energies of protons and neutrons are parametrized as a function of the primary particle energy and atomic number of target material [28]. The choice of energy E_{ca} is constrained to the interval

$$0 < \text{E}_{ca} \quad \text{T}_0 \quad \text{E}_{ex} \tag{8}$$

The excitation energy of target nucleus can be calculated from the condition

$$\text{E}_{ex} \quad \text{E} \quad \text{E}_{ca} \tag{9}$$

5. Selection of collision parameters and sites

Having cross sections of particle-particle interactions and a model for nuclear matter description, the choice of collision partners and collision sites can be done.

The probability of interaction (per 4-space unit) between one beam particles with momentum p_1 and volume density $_1$ and the second beam of particles with continuous momentum distribution is given by

$$P(\vec{p}_1) \quad _1 \quad _{12}(\vec{p}_2)\ _{12}(\vec{p}_2)\frac{^2}{d\vec{p}_2} d\vec{p}_2\ , \tag{10}$$

where the integration runs over the momentum distribution of the second beam. This situation is equivalent to the particle-nucleus interaction in the case when beam *1* represents the bombarding particles whereas the beam *2* consists of nucleons of the bombarded nucleus. The probability of interactions of the particle with laboratory velocity $_1$ with nucleon of the nucleus on the path of the unit length is

$$p \quad \frac{P(\vec{p}_1)}{_1} \quad \frac{1}{_1} \quad _{12}\ _2 \frac{^2}{d\vec{p}_2} d\vec{p}_2 \tag{11}$$

which is equal to the inverse value of the particle mean free path $(p \quad ^1)$. The probability of bombarding particle interaction within the interval $\langle l, l \quad dl \rangle$ is

$$dN(I) \quad e^{\ pl}\, pdl\,. \tag{12}$$

The complications connected with expression of $_{12}$ and $_{12}$ in a closed functional form lead to a numerical integration of formula (16). Taking into account the above presented nuclear model, the Fermi sphere of momentum was divided into n equal

$$p \quad \frac{1}{1} \sum_{i\ 1}^{n} {}^{(12)\,i} \quad {}^{(12)\,i} \quad {}^{i} \quad \frac{}{n} \sum_{i\ 1}^{n} {}^{i}\,, \tag{13}$$

where

$$\frac{{}^{(12)\,i}}{1} \quad {}^{(12)\,i}\,. \tag{14}$$

These equations are sufficient for the determination of the point of interaction and the collision partner. The procedure is as follows:

1. Determination whether a collision of the input particle with nucleon from nucleus has taken place in interval $\langle l,\ l \quad dl \rangle$. The probability of this event is given by integral of equation (17) which can be represented in analytical form

$$N(I) \quad 1 \quad \prod_{i\ 1}^{n} e^{\frac{l}{n}\ {}^{i}}, \tag{15}$$

where each term in the product is equivalent to the probability of no collision of the cascade particle with target nucleon in the interval l/n. The computer implementation of this step is based on indirect Monte Carlo integration of Equation (15) and comparison of the obtained value with the random number, which determines, whether the interaction has taken place. If the interaction has taken place, then

2. The site of collision is chosen.

3. The collision partner is chosen.

The step 2 is performed by division of the interval l into n equal subintervals and the probability of collision of the initial particle with a nucleon from nuclear Fermi gas with density and momentum $p_{\ i}$ is calculated for such subinterval $l_{\ l} \quad l/n$. The momentum of the target nucleon is chosen at random from momentum distribution corresponding to the nuclear spherical layer with constant density. After this choice the bombarding particle is shifted forward to a new position $l \quad dl$. Then the probability of collision of the bombarding particle with the target nucleon on the path is calculated. From the reason of simplification of calculation, saving the computer time and according to the fact that for small l and large enough n the relation $_{l}l/n \quad 1$ is correct, that allow us to use the linear approximation

$$N(l) \qquad {}_{i}\frac{1}{n} \tag{16}$$

for the probability of collision between the bombarding particle and the target nucleon in the interval $\langle l,\ l \quad dl \rangle$. This value is compared with the random number . If $N(\ ) \quad$, we claim that interaction has taken place. In the opposite case, the particle is only shifted forward and the whole procedure is repeated. In the case when the interaction took place in the interval $\langle l,\ l \quad dl \rangle$, the distance of the interaction point $x_{\ l}$ from the beginning of the interval l is determined. Using the relation (21) we have

$$x_i \quad {}_i / \quad {}_i \tag{17}$$

Then the calculations continue by the choice of the collision partner (Step 3), that is carried out by a rejection technique whereby a momentum p_l is chosen at random and probability of interaction with such a way characterized collision partner is compared with a second random number.

In the final part of the simulation, the reaction channel is chosen, the distributions of produced particles are constructed and their parameters are determined. In all the previous processes the particle reflection and refraction on the boundaries of regions with different densities are taken into account in the way described above.

The result of simulation is manifestly dependent on the choice of the size of interaction interval and on the number of subintervals n into which it is divided. The value of n is in general dependent on the accuracy and on the type and energy of the interacting particle.

The higher accuracy is required and the larger variation of cross sections are with energy, the larger n must be. The value of n is usually a compromise between the above listed requirements and constraints following from reasonable duration of computations. The first condition following from the accuracy requirement is the validity of approximation (4). From the requirement of good estimate of cascade development necessity of small l_i follows, which makes sure small changes in position of particle and its direction of motion. The mathematical formulation of the last condition leads to the requirement of good estimate of the integral (25) using the Monte Carlo method in the sense of the mean value estimate on some representative collection of generated cascades. The last condition can be fulfilled for smaller n, at required accuracy, by generation of a larger number of cascades. After the test calculations $n = 25$ was set as the compromise value.

The value of l was determined from the requirement of good estimate of probability p_l which leads to the value $\bar{l}$

$$\bar{l} \quad \frac{}{{}_{\max}} [Z \quad {}_p \quad (A \quad Z) \quad {}_n]^{1} \tag{18}$$

is the mean free path and ${}_{\max}$ is the total nucleon density. This equation has been corrected on resonance characteristics of ${}_n$ and ${}_p$.

6. Simulation of Evaporation processes

The excitation energy, which the nucleus acquires during cascade development, is distributed among nucleons. In any moment after the cascade stage this energy can be lowered by emission of additional particles. If this occurs earlier than steady state of nucleus is reached the characteristics of emitted particles are strongly influenced by the initial conditions. In other case, only conservation laws play the dominant role and the process is independent on the initial conditions. Our calculations are based on the model described by Dostrovsky et al. [6, 29].

The probability that i-type particle with the kinetic energy E_i will be emitted from the nucleus with the excitation energy E_{ex} is

$$P(E_i) \quad g_i m_i E_i \quad {}_{ci}(E_i) \quad (E \ ) \tag{19}$$

where g_i is the number of spin states, m_i is the emitted particle mass, $_{ci}$ is the inverse cross section, E is the excitation energy of the intermediate residual nucleus ($E \quad E_{ex} \quad Q \quad E_i$) where Q is the kinetic energy of i-type particle and is the energy level density of the residual nucleus.

The total (over all energy probability) of emission for each particle type is [31]

$$P_i \quad p_i / \quad _i p_i , \tag{20}$$

where

$$p_i \quad g_i m_i \quad \int_{k_i V_i}^{E_{ex} \quad Q_i} E_i \quad _{ci}(E_i) \ (E_{ex} \quad Q_i \quad E_i) dE_i , \tag{21}$$

where is the pairing energy and V_i is the Coulomb barrier. This expression is applicable only in the case $E_{ex} \quad k_i V_i \quad Q_i$, otherwise $P_i \quad 0$. This integral was calculated [29] for neutrons

$$P_i \quad A^{2/3} \quad [I_1(S) \quad I_0(S)] e^S \tag{22}$$

and for charged particles

$$P_i \quad (g_i m_i / 2)(1 \quad C_i) A^{2/3} I_1(S) e^S , \tag{23}$$

where

$$\begin{aligned} S \quad & 2[a(E_{ex} \quad k_i V_i \quad Q_i \quad]^{1/3} \\ I_0(S) \quad & (2a)^{\ 1}(S \quad 1 \quad e^{\ s}) \\ I_1(S) \quad & (8a^2)^{\ 1}(2S^2 \quad 6S \quad 6 \quad e^{\ s}(S^2 \quad 6)) \end{aligned} \tag{24}$$

and a is the parameter which characterizes the energy level density.

The cross sections of inverse reactions are taken to be the geometrical cross sections modified by the empirical experience with the aim to express their energy dependence and the influence of Coulomb barrier on charged particle emission. They were taken for neutron [31]

$$_{cn}(E_i) \quad R^2(1 \quad C_i)(1 \quad k_i V_i / E_i) , \tag{25}$$

where

$$\begin{aligned} & 0.76 \quad 1.93A^{\ 1/3} \\ & 1.66A^{\ 2/3} \quad 0.05 \\ R \quad & 1.7A^{1/3} \ fm \end{aligned} \tag{26}$$

and for charged particles

$$_{ci}(E_i) \quad R^2(1 \quad C_i)(1 \quad k_i V_i / E_i) \tag{27}$$

for $E_i \quad k_i V_i$ and 0 in the opposite case.

The energy level density is parameterized by expression

$$(E \ ) \quad e^{2[a(E \quad)]^{1/2}} , \tag{28}$$

where is the pairing energy again and according to [34]

$$a \quad a(A) \ 1 \quad \frac{f(E \ ) \quad _0(Y,A)}{E} , \tag{29}$$

where $a(A)$ corresponds to the asymptotic value of energy level density parameter at high excitation energy E and function $f(E)$ describes behavior of the parameter a at low energies and can be expressed as

$$f(E) \quad 1 \quad \exp(\quad E). \tag{30}$$

Parameter a was approximated as

$$a \quad A \quad A^{2/3}. \tag{31}$$

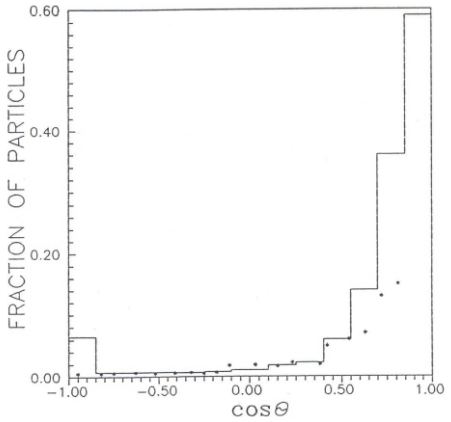

Fig. 2. Calculated angular distribution of protons emitted with energies greater than 90 MeV for the reaction of 1840 MeV protons on aluminum, experimental values (*) are from work [2].

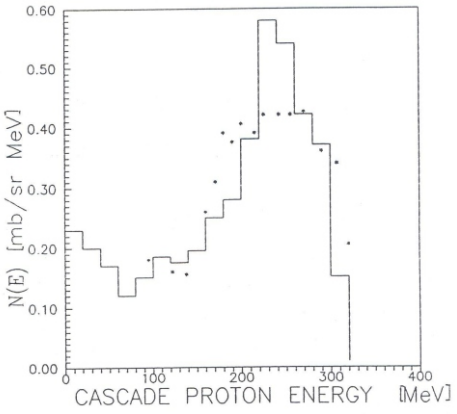

Fig. 3. Energy spectrum of cascade protons emitted at all angles for the reaction of 1840 MeV protons on aluminum. Experimental data (*) are from [2].

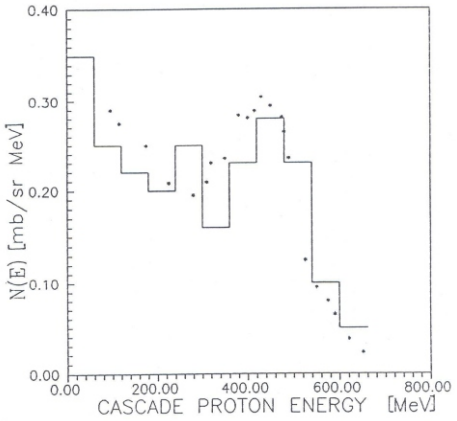

Fig. 4. Energy spectrum of cascade protons emitted at a laboratory angle 30° for the reaction of 340 MeV protons on carbon. Experimental values (*) are from [34] (the vertical scale for experimental data is arbitrary).

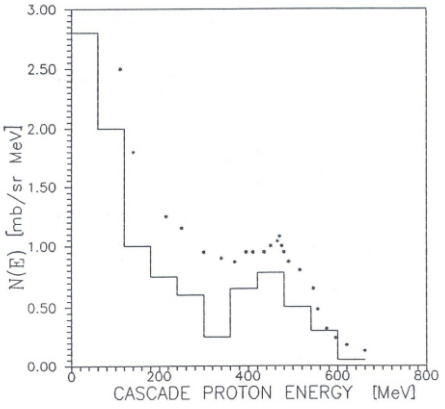

Fig. 5. Energy spectrum of cascade protons emitted at a laboratory angle 30° for the reaction of 660 MeV protons on carbon. Calculated data are for the angular interval 25–35° Experimental values (*) are from [35].

Using the expressions (29–31) the experimental data were analyzed and by least squares method the optimal values of coefficients , and were fixed. In our calculations, we used values = 0.114, = 0.162, and = 0.054 which give $a(A) = 1.47$.

The kinetic energy of emitted particle is determined from the distribution

$$N(E_i)dE_i \quad T_i^{\,2} W_i e^{\,W_i/T_i} dE_i , \tag{32}$$

where

$$W_i \quad E_i \quad k_i V_i$$
$$T_i \quad 1/2\langle W_i \rangle . \tag{33}$$

After the particle evaporation the whole procedure is repeated with changed characteristics of the nucleus

$$A \quad A \quad A_i$$
$$Z \quad Z \quad Z_i$$
$$E_{ex} \quad E_{ex} \quad Q_i \quad T_i . \tag{34}$$

7. Results and conclusions

This model was tested on calculations of basic characteristics of cascade and evaporation processes. Then it was applied to the calculation of cosmogenic nuclide production [32, 33].

In attempting to determine the difference in our results, comparisons were made with angular distribution, an energy spectrum and some of the nucleon multiplicities published previously. The initial conditions of our simulations were taken as those in the compared calculations. Therefore, differences in the results are presumably due to the resonance and pion production models. The other sources of differences in results of these calculations

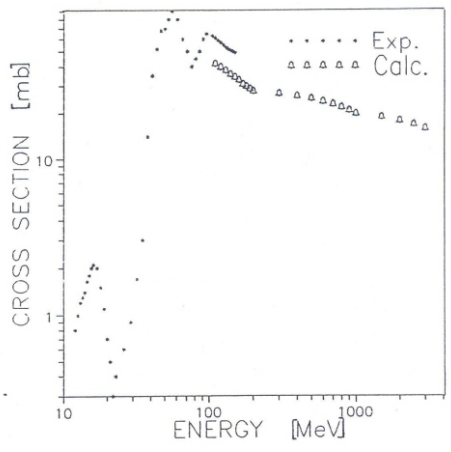

Fig. 6. Energy spectrum of cascade protons emitted at a laboratory angle 30° for the reaction of 660 MeV protons on uranium. Calculated data are for the angular interval 25–35° Experimental values (*) are from [35].

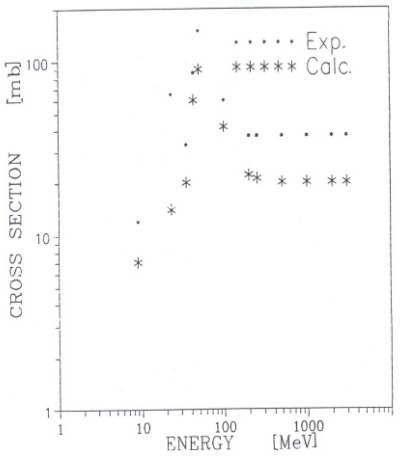

Fig. 7. Comparison of calculated and experimental [36, 37] excitation function Fe(p, 3pxn) ^{51}Cr.

are somewhat different elementary particle cross sections and a substantially different sampling technique employed for determining the type of reaction and properties of produced particles.

The results of our angular distribution calculations in Fig. 2 show a sharper forward peak than the previous calculations [2]. A quite good agreement was obtained between our and the previous calculations [2] of energy spectra of protons emitted from aluminum target (Fig. 3).

The secondary nucleon spectra were calculated for different energies. Fig. 4 illustrates the secondary cascade spectra at 30^{o} from 340 MeV protons on carbon. It is visible from the picture that the theoretical peak is somewhat sharper than that from the experiment [34]. That is in accordance with Bertini's calculations [16]. At wider angles the agreement between theoretical and measured values is better. Spectrum of the secondary particles produced at 30^{o} from 660 MeV protons with carbon is presented in Fig. 5. The shape of the theoretical spectrum is in a reasonable agreement with the experimental data, but the magnitude of the calculated values is systematically smaller than the measured ones. This conclusion is valid for simulations of all elements at this angle for 660 MeV proton beam. For smaller angles, the agreement is better. These conclusions are also confirmed by the data obtained from the uranium target (Fig. 6).

The first obvious quantity, which should be compared, is the reaction cross section predicted by each of the models. In our model, history of emitted particles (type, energy, momentum ...) and the history of residual nuclei (mass, charge, ...) are stored after each completely simulated reaction. After performing the predefined number of reactions, these data are analyzed. This analysis results in isobaric and isotopic yields of residual nuclides per incident source particle. By multiplication of these yields by the geometric cross section of the target nuclide, non-cumulative absolute production cross sections are obtained. The reliability and accuracy of the calculations depend strongly on the number of simulated reactions. Our calculations for 800 MeV protons agree with the experimental data within a factor of two (Tab. 1).

Table1. Comparison of the experimental [36] cross sections of some nuclear reactions induced by 600 MeV protons on iron targets with the values obtained by the presented model.

Reaction	Cross section	
	Experimental	Calculated
Fe(p, 2pxn)^{52}Mn	11.5 ± 0.6	24.5
Fe(p, 2pxn)^{54}Mn	39.8 ± 1.5	23.2
Fe(p, 3pxn)^{51}Cr	46.3 ± 1.7	23.4
Fe(p, xn)^{56}Co	1.36 ± 0,6	2.1

For comparison with the experimental data [36, 37], the excitation function for the reaction Fe(p, 3pxn)^{51}Cr is presented. The shape of the excitation function is described fairly well, but the calculated data are lower in comparison with the experimental ones by up to a factor of two. This situation can be improved by the inclusion of pre-equilibrium models in our cascade-evaporation model. This conclusion is the same as those in [36].

In general, the results of our calculations showed that the region of applicability of the cascade-evaporation model for simulation of nucleon-nucleus collisions is strongly restricted. The agreement of calculations with experimental data is at least within a factor of 2 and therefore there is the necessity to improve present model calculations.

Acknowledgements

One of the authors (J. M.) is indebted to P. Povinec, for many useful discussions and comments that helped to clarify a lot of points of the argumentation. I want to thank also my teachers M. Chudy, N. Pišútová, Š. Šáro and M. Florek for introducing me to the field of nuclear physics and especially computational nuclear physics.

References

[1] R. Serber: Phys. Rev. **72** (1947) 1114.
[2] N. Metropolis, R. Bivins, M. Storm, et al.: Phys. Rev. **110** (1958) 185.
[3] K. Chen, Z. Fraenkel, G. Friedlander, et al.: Phys. Rev. **166** (1868) 949.
[4] H. W. Bertini: Phys. Rev. **131** (1963) 1801.
[5] Y. Fujimoto, Y. Yamaguchi: Prog. Theor. Phys. **4** (1950) 468; **5** (1950) 787.
[6] I. Dostrovsky, P. Rabinowitz, R. Bivins: Phys. Rev. **111** (1958) 1659.
[7] V. S. Barashenkov, V. D. Toneev: Interaction of high-energy particles and atomic nuclei with nuclei, Moscow, Atomizdat (1972) 453 pp.
[8] J. W. Meadows: Phys. Rev. **98** (1955) 744.
[9] J. D. Jackson: Can. J. Phys. **35** (1957) 21.
[10] R. Hofstadter: Ann. Rev. Nucl. Sci. **7** (1957) 195.
[11] R. Kinsey: BNL-NCS-50496 (1979).
[12] A. Fumuro, R. Ibara, T. Ogata: Nucl. Phys. B**152** (1979) 376.
[13] D. Ashery, I. Avon, G. Azuelos et al.: Phys. Rev. C**23** (1981) 2173
[14] A. V. Vlasov, V. S. Vorobev. Y. G. Grishuk, et al.: Yad. Fyz. **27** (1978) 413.
[15] J. E. Elias, W. Busza, C. Haliwell, et al.: Phys. Rev. D**22** (1980) 13.
[16] H. W. Bertini: Phys. Rev. **188** (1969) 1711.
[17] E. Bracci, J. P. Droulaz, E. Falminio, et al.: CERN / HERA 73-1 (1973).
[18] O. Benari, N. Barash-Schmidt, L. R. Price, et al,: URL-200 Y.N. (1970).
[19] J. E. Enstrom, T. Ferbel, P.F. Slattery et al.: LBL-58 (1972).
[20] R. E. Heusmann: LBL-3030 (1972); LBL-3031 (1972).
[21] D. M. Chew, V. P. Henri, T. A. Lasinski, et al.: LBL-53 (1973).
[22] E. Flamino, J. D. Hansen, D. R. O. Morrison, et al.: CERN-HERA 70-5 (1970).
[23] U. Cassadei, G. Giacomelli, P. Lugaresi-Sera, et al.: CERN/HERA 75-1 (1975).
[24] U. Amaldi, M. Jacob, G. Mathiae: Rev. Nucl. Sci. **26** (1976) 385.
[25] R. M. Barnett, et al: Review of particle properties, Phys. Rev. D**54** (1996) 1.
[26] H. W. Bertini: ORNL-3383 (1963).
[27] K. Hansgen, J. Ranft: Comp. Phys. Comm. **39** (1986) 37.
[28] K. Hansgen, J. Ranft: Comp. Phys. Comm. **39** (1986) 53.
[29] I. Dobrovsky, Y. Fraenkel, C. Winsbert: Phys. Rev. **118** (1960) 781.
[30] I. Dobrovsky, Y. Fraenkel, G. Friedlander: Phys. Rev. **116** (1959) 683.
[31] P. Cloth, D. Filges, R. D. Neef et al.: Jul **2203** (1988).
[32] J. Masarik, P. emrich, P. Povinec, et al.: Nucl. Instrum. Meth. B**17** (1986) 483.
[33] J. Masarik, P. Chochula, P. Povinec: J. Phys. G**17** (1991) S493.
[34] J. B. Chadis, W. N. Hess, B. J. Mayer: Phys. Rev. **87** (1952) 425.
[35] L. S. Azhgirey, J. K. Vzorov: Nucl. Phys. **13** (1959) 258/
[36] R. Michel, B. Dittrich, U. Herpers, et al.: Analyst **114** (1989) 287.
[37] G. M. Raisbeck, F. Yiou: Proc. 14th ICRC Vol. **2** (1975) 495.